Journal of Science and Transport Technology
Journal homepage: https://jstt.vn/index.php/en

Nonlinear buckling and postbuckling analysis of cylindrical and sinusoid FG-GPLRC panels under axial compressive load

Dao Quang Huy[1], Nguyen Thi Phuong[2,3,*]

[1]Faculty of Civil Engineering, University of Transport Technology, Hanoi 10000, Vietnam

[2]Laboratory of Advanced Materials and Structures, Institute for Advanced Study in Technology, Ton Duc Thang University, Ho Chi Minh City 70000, Vietnam

[3]Faculty of Civil Engineering, Ton Duc Thang University, Ho Chi Minh City 70000, Vietnam

Article info
Type of article:
Original research paper

DOI:
https://doi.org/10.58845/jstt.utt.2023.en.3.3.44-53

***Corresponding author:**
E-mail address:
nguyenthiphuong@tdtu.edu.vn

Received: 11/09/2023
Revised: 27/09/2023
Accepted: 29/09/2023

Abstract: This paper presents and analyzes the nonlinear buckling responses of cylindrical and sinusoid Functionally graded graphene platelet reinforced composite (FG-GPLRC) panels under axial compressive load. The higher-order shear deformation theory is applied to establish the governing equations of structures. The stress function is approximated using the like-Galerkin method, and the Galerkin method is applied to solve the governing equations. The critical buckling loads and postbuckling load-deflection curves are expressed in explicit form. The effects of panel types, geometrical parameters, imperfection, and foundation on the critical buckling loads and postbuckling curves of cylindrical and sinusoid FG-GPLRC panels are discussed. Numerical results also evaluate and compare the buckling responses of cylindrical and sinusoid panels.

Keywords: Graphene platelet reinforced composite; Elastic foundation; Sinusoid panel; Cylindrical panel; Buckling and Postbuckling.

1. Introduction

The functionally graded composite material (FGM) is an advanced composite material, with significant importance in technology industries. The excellent thermo-mechanical properties of FGM are the high resistance strength, high moduli, and low extension and heat transfer coefficients. Many authors focused on the FGM plates and cylindrical panels using different theories and methods, for linear buckling problems [1-2], and nonlinear thermal postbuckling problems [3]. The FGM plates reinforced by orthogonal and oblique stiffeners were investigated and disused using higher-order shear deformation theory (HSDT) [4,5]. More complex FGM structures such as cylindrical panels and doubly curved shallow shells are also mentioned in many publications [6,7].

The functionally graded carbon nanotubes reinforced composite (FG-CNTRC) is formed by combining a polymer matrix and a reinforced material, carbon nanotube (CNT), with the volume fraction of CNT changing linearly, smoothly, and continuously from one side to the other of structures. The thermomechanical properties of the matrix material are largely improved. The thermo-mechanical behavior of FG-CNTRC plates was

studied for nonlinear thermal buckling and postbuckling problems [8], nonlinear mechanical postbuckling and buckling problems [9,10], and linear vibration problems [11].

With excellent thermomechanical characteristics, graphene material has considerably drawn the attention of numerous expert researchers in recent years. Graphene is also an excellent reinforcement for polymer matrix. The functionally graded graphene reinforced composite (FG-GRC) is also formed by combining a polymer matrix and graphene sheets with the volume fraction of graphene changing piecewisely in the thickness direction of structures. The mechanical buckling, thermal buckling, and vibration problems of FG-GRC laminated plates were studied [12-14] by using the two-step perturbation technique. Thermal postbuckling, vibration, and multi-scale buckling problems of FG-GRC laminated plates were also investigated using NURBS formulation and the incremental-iterative type of the Ritz method [15-17]. The electro-mechanical behavior of FG-GRC plates with the piezoelectric actuator was investigated using the finite element method [18]. Nonlinear buckling of FG-GRC higher-order shear deformable plates and cylindrical panels were investigated using the Galerkin method [19-22]. The buckling and postbuckling behavior of FG-GRC panels under external pressure and axial compression with complex curvatures such as parabola and sinusoid panels were also studied [23,24].

Next, functionally graded graphene platelet reinforced composite (FG-GPLRC) is also an advanced composite material, with advantages in ease of fabrication compared to FG-CNTRC and FG-GRC. The buckling, bending, and vibration behavior of FG-GPLRC plates and shells were mentioned in many publications [25-29].

In this paper, the HSDT is used and the approximate technique to determine the stress function is applied. The problems are solved using the Galerkin method, and the critical loads and postbuckling curves are obtained. Influences of material parameters of FG-GPLRC, elastic foundation, and geometrical parameters on the buckling and postbuckling responses of the FG-GPLRC cylindrical and sinusoid panels are investigated and discussed.

2. Material and Geometrical properties of FG-GPLRC panels, governing equations, and solving problems

An FG-GPLRC panel with a shallow curvature in the y-direction is considered. The panel is under axial compressive load P_x (in Pa). R, a, b and h are respectively the radius, longitudinal and circumferential lengths, and panel thickness. The coordinate system of panels is applied as in Figure 1, where the shallowness approximation is applied to simplify the cylindrical system to a Cartesian system. The panel rests on the Pasternak's elastic foundation with the two foundation stiffnesses K_1 and K_2.

The Young's modulus of FG-GPLRC panels is determined based on the extended Halpin-Tsai model as follows [26].

$$E(z)=\left(\frac{3}{8}\frac{1+\zeta_1\delta_1 V_{GPL}}{1-\delta_1 V_{GPL}}+\frac{5}{8}\frac{1+\zeta_2\delta_2 V_{GPL}}{1-\delta_2 V_{GPL}}\right)E_{m,} \quad (1)$$

where

$$\delta_1=\frac{(E_{GPL}/E_m)-1}{(E_{GPL}/E_m)+\zeta_1},\ \zeta_1=2\left(\frac{a_{GPL}}{t_{GPL}}\right),$$
$$\delta_2=\frac{(E_{GPL}/E_m)-1}{(E_{GPL}/E_m)+\zeta_2},\ \zeta_2=2\left(\frac{b_{GPL}}{t_{GPL}}\right), \quad (2)$$

with E_m and E_{GPL} are respectively the elastic moduli of the matrix and graphene platelet (GPL), a_{GPL}, b_{GPL} and t_{GPL} are the length, width and thickness of the GPL, respectively.

The volume fraction V_{GPL} of the GPL $(V_m+V_{GPL}=1)$, defined as [26]

$$V_{GPL}(z)=\frac{W_{GPL}}{W_{GPL}+(\rho_{GPL}/\rho_m)(1-W_{GPL})}, \quad (3)$$

where ρ_m and ρ_{GPL} are the densities of the matrix and the GPL, respectively.

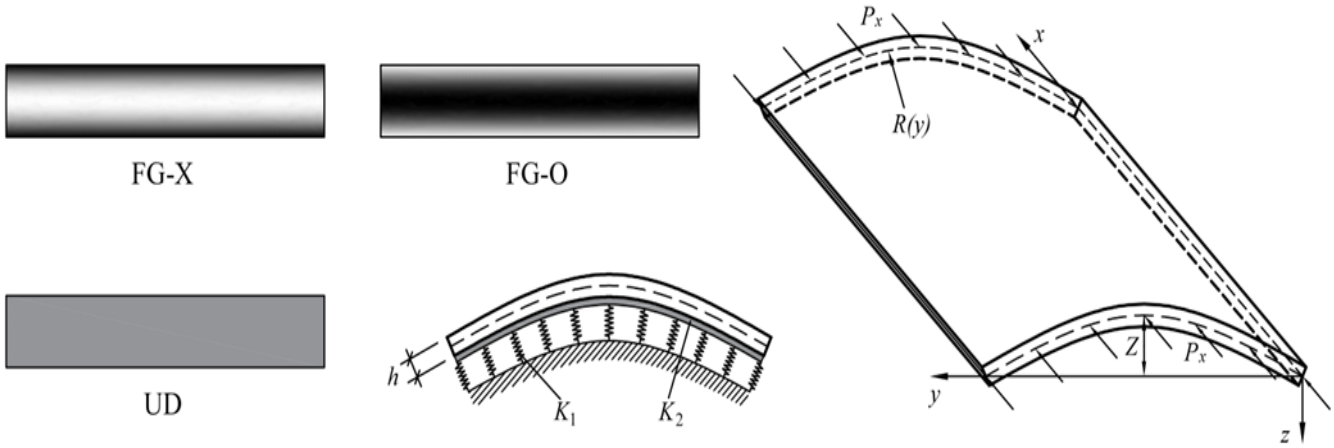

Fig 1. Configuration of FG-GPLRC panels under axial compressive load

The mass fraction W_{GPL} of GPL depends on three popular distribution laws of GPL of panels with the following functions [26]

$$W_{GPL}(z)=\begin{cases} W^{*}_{GPL} \text{ for UD-GPLRC,} \\ 4\dfrac{|z|}{h}W^{*}_{GPL} \text{ for FG-X-GPLRC,} \\ 2\left(1-\dfrac{2|z|}{h}\right)W^{*}_{GPL} \text{ for FG-O-GPLRC,} \end{cases} \quad (4)$$

where W^{*}_{GPL} denotes the total mass fraction of GPL, and $(-h/2 \le z \le h/2)$.

According to the rule of mixture, the Poisson's ratio is determined as [26]

$$\nu(z)=\nu_m(1-V_{GPL})+\nu_{GPL}V_{GPL}, \quad (5)$$

The configuration equations for the middle surface in the y-direction are respectively written for sinusoid panels, as

$$z=-Z\sin(\pi y/b), \quad (6)$$

The radius R of the sinusoid panels is determined, as

$$R=\frac{\left\{\left[Z\pi\cos(y\pi/b)\right]^2+b^2\right\}^{3/2}}{bZ\pi^2\sin(y\pi/b)} \quad (7)$$

For cylindrical panels, R is a constant.

The HSDT is applied to formulate the basic equation system of structures. The strain-displacement relations considering the von Karman nonlinearities and imperfection function w_0 are

$$\begin{Bmatrix}\varepsilon_x\\ \varepsilon_y\\ \gamma_{xy}\end{Bmatrix}=\begin{Bmatrix}\varepsilon_{0x}\\ \varepsilon_{0y}\\ \gamma_{0xy}\end{Bmatrix}+z\begin{Bmatrix}\phi_{x,x}\\ \phi_{y,y}\\ \phi_{y,x}+\phi_{x,y}\end{Bmatrix} -\frac{4}{3}z^3h^2\begin{Bmatrix}w_{,xx}+\phi_{x,x}\\ w_{,yy}+\phi_{y,y}\\ \phi_{x,y}+2w_{,xy}+\phi_{y,x}\end{Bmatrix}, \quad (8)$$

$$\begin{Bmatrix}\gamma_{xz}\\ \gamma_{yz}\end{Bmatrix}=\begin{Bmatrix}\gamma_{0xz}\\ \gamma_{0yz}\end{Bmatrix}-4z^2h^2\begin{Bmatrix}w_{,x}+\phi_x\\ w_{,y}+\phi_y\end{Bmatrix},$$

with

$$\begin{Bmatrix}\varepsilon_{0x}\\ \varepsilon_{0y}\\ \gamma_{0xy}\\ \gamma_{0xz}\\ \gamma_{0yz}\end{Bmatrix}=\begin{Bmatrix}u_{,x}+\dfrac{w_{,x}^2}{2}+w_{,x}w_{0,x}\\ v_{,y}+\dfrac{w_{,y}^2}{2}+w_{,y}w_{0,y}-\dfrac{w}{R}\\ \left(v_{,x}+u_{,y}+w_{,x}w_{,y}\right.\\ \left.+w_{,y}w_{0,x}+w_{,x}w_{0,y}\right)\\ w_{,x}+\phi_x\\ w_{,y}+\phi_y\end{Bmatrix}, \quad (9)$$

where $\varepsilon_{0xx},\varepsilon_{0yy},\gamma_{0xy},\gamma_{0xz},\gamma_{0yz}$ are the strains at mid-plane of panels.

The relations between internal forces with the strains, rotations, and deflection are obtained as

$$\begin{Bmatrix} N_x \\ N_y \\ N_{xy} \\ M_x \\ M_y \\ M_{xy} \\ T_x \\ T_y \\ T_{xy} \end{Bmatrix} = \begin{bmatrix} B_{11} & B_{12} & 0 & D_{11} & D_{12} & 0 & F_{11} & F_{12} & 0 \\ B_{12} & B_{22} & 0 & D_{12} & D_{22} & 0 & F_{12} & F_{22} & 0 \\ 0 & 0 & B_{66} & 0 & 0 & D_{66} & 0 & 0 & F_{66} \\ D_{11} & D_{12} & 0 & E_{11} & E_{12} & 0 & H_{11} & H_{12} & 0 \\ D_{12} & D_{22} & 0 & E_{12} & E_{22} & 0 & H_{12} & H_{22} & 0 \\ 0 & 0 & D_{66} & 0 & 0 & E_{66} & 0 & 0 & H_{66} \\ F_{11} & F_{12} & 0 & H_{11} & H_{12} & 0 & I_{11} & I_{12} & 0 \\ F_{12} & F_{22} & 0 & H_{12} & H_{22} & 0 & I_{12} & I_{22} & 0 \\ 0 & 0 & F_{66} & 0 & 0 & H_{66} & 0 & 0 & I_{66} \end{bmatrix} \begin{Bmatrix} \varepsilon_{0x} \\ \varepsilon_{0y} \\ \gamma_{0xy} \\ \phi_{x,x} \\ \phi_{y,y} \\ \phi_{x,y} + \phi_{y,x} \\ -\lambda\left(\phi_{x,x} + w_{,xx}\right) \\ -\lambda\left(\phi_{y,y} + w_{,yy}\right) \\ -\lambda\left(2w_{,xy} + \phi_{x,y} + \phi_{y,x}\right) \end{Bmatrix}, \tag{10}$$

The shear and higher-order shear forces can be obtained as

$$\begin{aligned} &J_x = K_{44}w_{,x} + K_{44}\phi_x,\ J_y = K_{55}w_{,y} + K_{55}\phi_y, \\ &S_x = K_{66}w_{,x} + K_{66}\phi_x,\ S_y = K_{77}w_{,y} + K_{77}\phi_y, \end{aligned} \tag{11}$$

The compatibility equation can be determined as

$$\begin{aligned} &\varepsilon_{0xx,yy} + \varepsilon_{0yy,xx} - \gamma_{0xy,xy} = w_{,xy}^2 - w_{0,xx}w_{,yy} \\ &-\frac{w_{,xx}}{R} - w_{,xx}w_{,yy} - w_{,xx}w_{0,yy} + 2w_{,xy}w_{0,xy}. \end{aligned} \tag{12}$$

The equilibrium equation system of the FG-GPLRC panels under axial compressive load is obtained as

$$\begin{aligned} &N_{x,x} + N_{xy,y} = 0,\ N_{xy,x} + N_{y,y} = 0, \\ &J_{y,y} + J_{x,x} - 3\lambda\left(S_{x,x} + S_{y,y}\right) \\ &+\lambda\left(T_{x,xx} + 2T_{xy,xy} + T_{y,yy}\right) + \frac{N_y}{R} \\ &+N_x\left(w_{,xx} + w_{0,xx}\right) + 2\left(w_{,xy} + w_{0,xy}\right)N_{xy} \\ &+N_y\left(w_{,yy} + w_{0,yy}\right) - K_1 w + K_2\nabla^2 w = 0, \\ &M_{x,x} + M_{xy,y} - \lambda\left(T_{x,x} + T_{xy,y} - 3S_x\right) - J_x = 0, \\ &M_{xy,x} + M_{y,y} - \lambda\left(T_{xy,x} + T_{y,y} - 3S_y\right) - J_y = 0. \end{aligned} \tag{13}$$

The stress function Γ can be introduced as

$$N_x = \Gamma_{,yy},\ N_y = \Gamma_{,xx},\ N_{xy} = -2\Gamma_{,xy}. \tag{14}$$

Substituting Eqs. (10) , (11) and (14) into the last three equations of Eq. (13), yields the following equations

$$\begin{aligned} &-\lambda F_{21}^{*}\Gamma_{,xxxx} + v_1\Gamma_{,xxyy} - \lambda F_{12}^{*}\Gamma_{,yyyy} \\ &-\frac{16}{9}h^4 I_{11}^{*}w_{,xxxx} + v_2 w_{,xxyy} + v_3\phi_{x,xxx} \\ &+v_4\phi_{x,xyy} + v_5\phi_{y,xxy} - \frac{16}{9}h^4 I_{22}^{*}w_{,yyyy} \\ &+v_7\phi_{x,x} + \left(w_{,yy} + w_{0,yy}\right)\Gamma_{,xx} + v_6\phi_{y,yyy} \\ &+\left(v_7 + K_2\right)w_{,xx} + \left(w_{,xx} + w_{0,xx}\right)\Gamma_{,yy} \\ &-2\left(w_{,xy} + w_{0,xy}\right)\Gamma_{,xy} + v_8\phi_{y,y} + \frac{\Gamma_{,xx}}{R} \\ &+\left(v_8 + K_2\right)w_{,yy} - K_1 w = 0, \end{aligned} \tag{15}$$

$$\begin{aligned} &q_1\Gamma_{,xxx} + q_2\Gamma_{,xyy} + q_3 w_{,xxx} + q_4 w_{,xyy} \\ &+q_5\phi_{x,xx} + q_6\phi_{x,yy} + q_7\phi_{y,xy} + q_8 w_{,x} \\ &+3\lambda K_{66}\phi_x - K_{44}\phi_x = 0, \end{aligned} \tag{16}$$

$$\begin{aligned} &h_1\Gamma_{,xxy} + h_2\Gamma_{,yyy} + h_3 w_{,xxy} + h_4 w_{,yyy} \\ &+h_8 w_{,y} + h_5\phi_{x,xy} + h_7\phi_{y,yy} + h_6\phi_{y,xx} \\ &+3\lambda K_{77}\phi_y - K_{55}\phi_y = 0, \end{aligned} \tag{17}$$

The new form of compatibility equation can be obtained by substituting Eq. (10) into Eq. (12), and then taking into account Eq. (14), as

$$\begin{aligned} &\Theta \equiv B_{11}^{*}\Gamma_{,xxxx} + B_{22}^{*}\Gamma_{,yyyy} + e_1\Gamma_{,xxyy} \\ &+\frac{w_{,xx}}{R} + w_{,xx}w_{,yy} + w_{,xx}w_{0,yy} - \left(w_{,xy}\right)^2 \\ &+w_{,yy}w_{0,xx} - 2w_{,xy}w_{0,xy} - \lambda F_{21}^{*}w_{,xxxx} \\ &-\lambda F_{12}^{*}w_{,yyyy} + e_2 w_{,xxyy} + e_4\phi_{x,xyy} \\ &+e_6\phi_{y,yyy} + e_5\phi_{y,xxy} + e_3\phi_{x,xxx} = 0, \end{aligned} \tag{18}$$

The simply supported and freely movable boundary condition is considered at all edges, as

$$\begin{aligned} &M_y\big|_{y=0,b}=0,\ w\big|_{y=0,b}=0,\quad N_{xy}\big|_{y=0,b}=0,\\ &\phi_x\big|_{y=0,b}=0,\ T_y\big|_{y=0,b}=0,\ N_y=N_{y0}=0,\\ &M_x\big|_{x=0,a}=0,\ w\big|_{x=0,a}=0,\ N_{xy}\big|_{x=0,a}=0,\\ &\phi_y\big|_{x=0,a}=0,\ T_x\big|_{x=0,a}=0,\ N_x=N_{x0}=-hP_x, \end{aligned} \tag{19}$$

The analytical solutions can be chosen in approximate forms, as

$$\begin{aligned} &w=W\sin\beta x\sin\gamma y,\phi_x=\Phi_x\cos\beta x\sin\gamma y,\\ &\phi_y=\Phi_y\sin\beta x\cos\gamma y,w_0=h\varsigma\sin\beta x\sin\gamma y \end{aligned} \tag{20}$$

where ς is the imperfection size, $\beta=\pi m/a$, $\gamma=\pi n/b$ with m and n are the buckling modes of panels.

The approximate stress function is chosen to be the same form as the exact form of cylindrical panels [21,22], as

$$\begin{aligned} \Gamma=&\Gamma_1\sin\beta x\sin\gamma y+\Gamma_2\cos 2\beta x\\ &+\Gamma_3\cos 2\gamma y+x^2\frac{N_{y0}}{2}+y^2\frac{N_{x0}}{2}, \end{aligned} \tag{21}$$

The parameters of the stress function can be obtained by substituting Eqs. (20) and (21) into Eq. (18), and applying the like-Galerkin method, as

$$\begin{aligned} &\int_0^b\int_0^a\Theta\cos 2\beta x\,dxdy\\ &=\int_0^b\int_0^a\Theta\cos 2\gamma y\,dxdy\\ &=\int_0^b\int_0^a\Theta\sin\beta x\sin\gamma y\,dxdy=0. \end{aligned} \tag{22}$$

Substituting Eqs. (20) and (21) into the Eqs. (15-17), and then applying the Galerkin procedure for the resulting equations yields

$$\begin{aligned} &y_1N_{x0}(\varsigma h+W)+y_2N_{y0}(\varsigma h+W)+y_{11}N_{y0}\\ &+y_3\Phi_x+y_{12}W+y_7W^3+y_9W(2\varsigma h+W)\\ &+y_6(\varsigma h+W)\Phi_y+y_8W(2\varsigma h+W)(\varsigma h+W)\\ &+y_5(\varsigma h+W)\Phi_x+y_{10}W(\varsigma h+W)+y_4\Phi_y=0, \end{aligned} \tag{23}$$

$$c_1\Phi_x+c_2\Phi_y+c_4W+c_3(2\varsigma h+W)W=0, \tag{24}$$

$$c_5\Phi_x+c_6\Phi_y+c_8W+c_7(2\varsigma h+W)W=0, \tag{25}$$

Solving Φ_x,Φ_y from Eqs. (24), (25), then substituting the obtained results with $N_{x0}=-hP_x$ into Eq. (23), the expression of the postbuckling curve can be obtained

$$P_x=\frac{y_7\bar{W}^3h^2+a_8\bar{W}+a_5(2\varsigma+\bar{W})\bar{W}+a_7\bar{W}(\varsigma+\bar{W})+a_6(2\varsigma+\bar{W})\bar{W}(\xi+\bar{W})}{hx_1(\varsigma+\bar{W})}, \tag{26}$$

where $\bar{W}=W/h$.

By applying $\bar{W}\to 0$ into Eq. (26), the expression of the critical buckling compressive load of perfect FG-GPLRC cylindrical and sinusoid panels can be obtained as

$$P_{cr}=-\frac{a_8}{x_1h}, \tag{27}$$

3. Numerical examples

The results of FGM cylindrical panels are compared with those of Bich et al. [6] and Dung and Dong [7] to verify the accuracy of the present work in Table 1. The work of Bich et al. [6] used the nonlinear classical shell theory (CST), meanwhile, Dung and Dong [7] used the HSDT.

The comparison shows that good agreements can be observed.

In this paper, the material parameters of FG-GPLRC are chosen according to the work of Wang et al. [26]. The critical compressive loads of the FG-GPLRC cylindrical and sinusoid panels with different GPL distribution laws and different weight fractions of GPL are presented in Table 2. The significant differences in the critical buckling loads can be obtained with the different distribution laws.

Additionally, the large effects of the weight fraction of GPL can be observed in this table. The critical buckling compressive loads strongly increase with only the addition of 1% mass fraction of GPL. The FG-X distribution law shows the superiority of the critical buckling load of the FG-GPLRC panels, and this superiority can be more clearly observed as the mass fraction of GPL increases.

Table 1. Comparison of critical loads of FGM cylindrical panels with the previous works (10^8N.m^{-2})

a/h	Bich et al. [6] (CST)	Dung and Dong [7] (HSDT)	Present
100	9.85	9.84	9.84
90	10.80	10.78	10.78
60	16.13	16.10	16.10
50	19.52	19.44	19.44
40	25.70	25.53	25.53
30	39.07	38.52	38.52
20	77.26	74.54	74.54
10	283.50	244.58	244.58

Table 2. Critical compressive load (GPa) of FG-GPLRC panels (h=0.01m, $a=b=20h$, $Z=1.5h$, ς=0, $m=n=1$, K_1= 50 MN/m^3, K_2 = 0.5 MN/m)

Type		W^*_{GPL}				
		0%	0.25%	0.5%	0.75%	1%
UD	Sinusoid panel	2.482	2.809	3.123	3.426	3.717
	Cylindrical panel	2.445	2.767	3.076	3.374	3.661
FG-X	Sinusoid panel	2.482	2.884	3.264	3.623	3.963
	Cylindrical panel	2.445	2.842	3.217	3.571	3.907
FG-O	Sinusoid panel	2.482	2.728	2.964	3.190	3.407
	Cylindrical panel	2.445	2.686	2.917	3.139	3.351

Postbuckling curves of FG-GPLRC panels with cylindrical and sinusoid cases are presented in Fig. 2a. A slight advantage of sinusoid panels in critical buckling load over cylindrical panels can be observed, however, the snap-through intensity of sinusoid FG-GPLRC panels is slightly greater than that of cylindrical FG-GPLRC panels. Effects of geometrical parameters of UD and FG-O panels on the postbuckling curves are presented in Figs. 2b,c. The postbuckling strength of panels strongly increases when the a/h ratio decreases, however, the snap-through phenomenon also strongly increases. The rise of the FG-GPLRC panels strongly affects the upper critical buckling load of the panels, however, the critical buckling load does not change much when changing the rise (Fig. 2c). Figure 2d presents the effects of the distribution laws of GPL on the postbuckling curves of sinusoid FG-GPLRC panels. Similar to the results of critical buckling loads, the postbuckling strength of the FG-X panel is also overwhelmingly dominant. The tendencies of postbuckling curves of panels with three distribution laws are quite similar. A large amount of GPL is distributed far from the middle surface, causing the stiffnesses to increase, leading to a significant increase in the load-bearing capacity of panels

Effects of the mass fraction of GPL on the nonlinear postbuckling strength of the sinusoid FG-GPLRC panel are presented in Fig. 2e. Clearly, the postbuckling strength of the panel increases largely when the mass fraction of GPL increases,

and it seems that the insignificant change in snap-through intensity of FG-GPLRC panels can be observed. Of course, the higher the mass fraction of GPL, the higher the panel's elastic modulus, leading to a higher load-bearing capacity of the panel.

Effects of elastic foundation and imperfection size on the postbuckling strength of cylindrical FG-GPLRC panels are presented in Fig. 2f. As can be seen the postbuckling curve is upper with larger values of foundation parameters. The imperfection of panels also strongly influences the postbuckling curve. Due to the imperfection of the panel, the membrane state of the panel does not appear, leading to no branching phenomenon for the imperfect panel. In addition, the snap-through phenomenon strongly decreases with the imperfect panels.

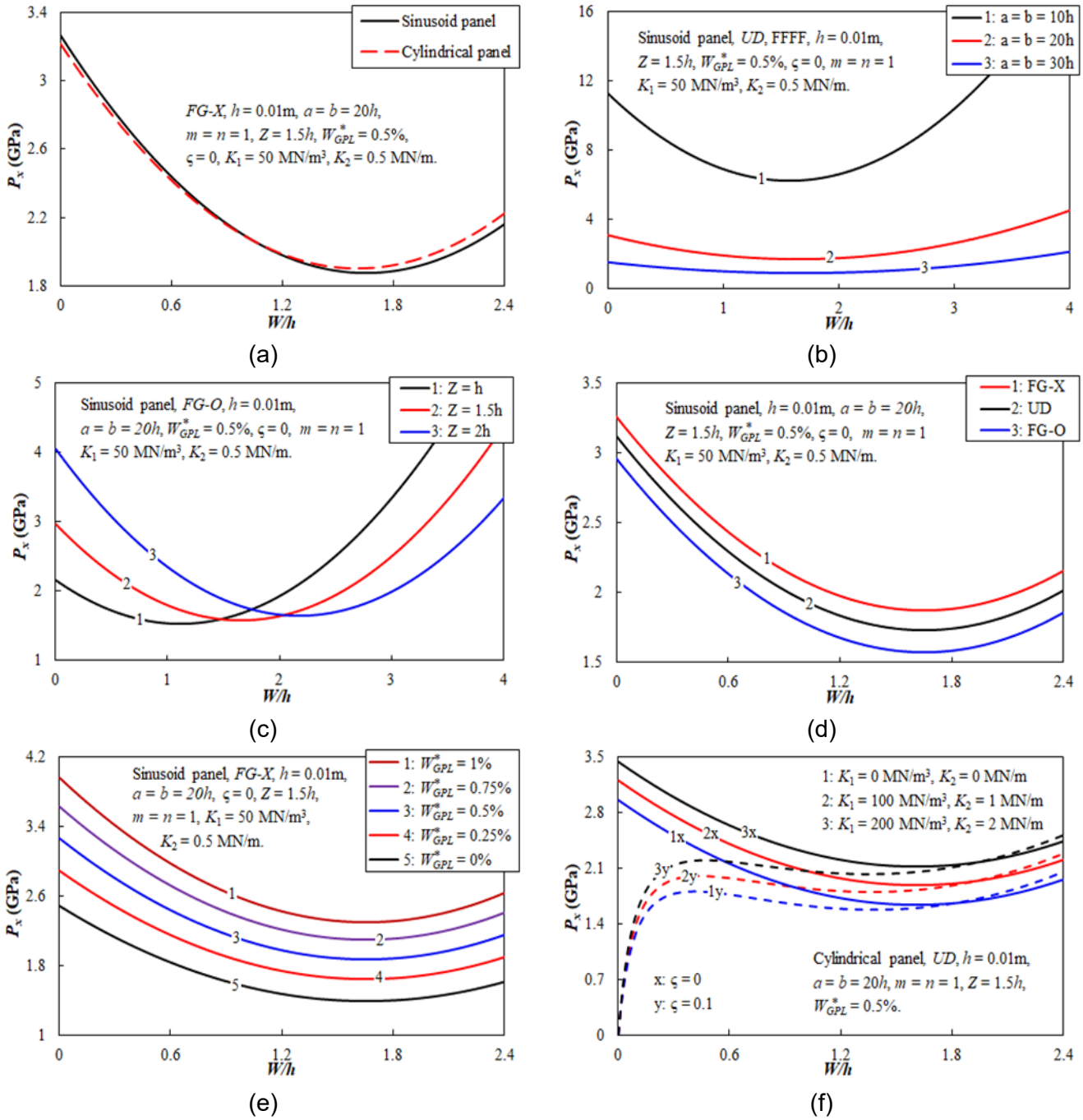

Fig. 2. Effects of panel type, mass fractions and distribution laws of GPL, geometrical parameters, and elastic foundation on the postbuckling curves

4. Conclusion

This paper presents an analytical approach to the nonlinear buckling of FG-GPLRC cylindrical and sinusoid panels. The HSDT and Galerkin method are applied and the formula of the critical loads and postbuckling curves are obtained. The stress function is introduced and determined using an approximate technique. Numerical examples present the increase of the GPL mass fraction causes the critical buckling loads and postbuckling behavior to increase for both three distribution laws of UD, FG-X, and FG-O. A slight advantage of sinusoid panels in critical buckling load over cylindrical panels can be observed, however, the snap-through phenomenon of sinusoid FG-GPLRC panels is slightly greater than that of cylindrical FG-GPLRC panels. In addition, the large effects of material and geometrical parameters on the buckling behavior of panels can be observed from the numerical investigations.

References

[1] A.M.A. Zenkour. (2005). Comprehensive analysis of functionally graded sandwich plates: Part 2-Buckling and free vibration. *International Journal of Solids and Structures*, 42(18-19) 5243-5258.

[2] B.A.S. Shariat, R. Javaheri, M.R. Eslami. (2005). Buckling of imperfect functionally graded plates under in-plane compressive loading. *Thin-Walled Structures*, 43(7), 1020-1036.

[3] H.S. Shen. (2007). Thermal postbuckling behavior of shear deformable FGM plates with temperature-dependent properties. *International Journal of Mechanical Sciences*, 49(4), 466-478.

[4] V.H. Nam, N.T. Phuong, D.T. Dong, N.T. Trung, N.V. Tue. (2019). Nonlinear thermo-mechanical buckling of higher-order shear deformable porous functionally graded material plates reinforced by orthogonal and/or oblique stiffeners. *Proceedings of the Institution of Mechanical Engineers, Part C: Journal of Mechanical Engineering Science*, 233(17), 6177-6196.

[5] D.T. Dong, V.H. Nam, N.T. Trung, N.T. Phuong, V.T. Hung. (2020). Nonlinear thermomechanical buckling of sandwich FGM oblique stiffened plates with nonlinear effect of elastic foundation. *Journal of Thermoplastic Composite Materials*, 35(10), 1441-1467.

[6] D.H. Bich, D.V. Dung, V.H. Nam. (2012). Nonlinear dynamical analysis of eccentrically stiffened functionally graded cylindrical panels. *Composite Structures*, 94(8), 2465-2473.

[7] D.V. Dung, D.T. Dong. (2017). Nonlinear thermo-mechanical stability of eccentrically stiffened functionally graded material sandwich doubly curved shallow shells with general sigmoid law and power law according to third-order shear deformation theory. *Applied Mathematics and Mechanics*, 38, 191-216.

[8] H.S. Shen, C.L. Zhang. (2010). Thermal buckling and postbuckling behavior of functionally graded carbon nanotube-reinforced composite plates. *Materials & Design*, 31(7), 3403-3411.

[9] H.S. Shen, Z.H. Zhu. (2012). Postbuckling of sandwich plates with nanotube-reinforced composite face sheets resting on elastic foundations. *European Journal of Mechanics - A/Solids*, 35, 10-21.

[10] L.W. Zhang, K.M. Liew. (2016). Postbuckling analysis of axially compressed CNT reinforced functionally graded composite plates resting on Pasternak foundations using an element-free approach. Composite Structures, 138, 40-51.

[11] L.W. Zhang, W.C. Cui, K.M. Liew. (2015). Vibration analysis of functionally graded carbon nanotube reinforced composite thick plates with elastically restrained edges. *International Journal of Mechanical Sciences*, 103, 9-21.

[12] H.S. Shen, Y. Xiang, F. Lin, D. Hui. (2017). Buckling and postbuckling of functionally graded graphene-reinforced composite laminated plates in thermal environments.

Composites Part B: Engineering, 119, 67-78.

[13] Y. Fan, Y. Xiang, H.S. Shen. (2019). Nonlinear forced vibration of FG-GRC laminated plates resting on visco-Pasternak foundations. *Composite Structures*, 209, 443-452.

[14] H.S. Shen, Y. Xiang, J.N. Reddy. (2019). Thermal postbuckling behavior of FG-GRC laminated cylindrical panels with temperature-dependent properties. *Composite Structures*, 211, 433-442.

[15] Y. Kiani. (2018). NURBS-based isogeometric thermal postbuckling analysis of temperature dependent graphene reinforced composite laminated plates. *Thin-Walled Structures*, 125, 211-219.

[16] Y. Kiani. (2018). Isogeometric large amplitude free vibration of graphene reinforced laminated plates in thermal environment using NURBS formulation. *Computer Methods in Applied Mechanics and Engineering*, 332, 86-101.

[17] M.K. Zeverdejani, Y.T. Beni, Y. Kiani. (2020). Multi-Scale buckling and post-buckling analysis of functionally graded laminated composite plates reinforced by defective graphene sheets. *International Journal of Structural Stability and Dynamics*, 20(1), 2050001.

[18] Q. Jin. (2022). A new electro-mechanical finite formulation for functionally graded graphene reinforced composite laminated thick plates with piezoelectric actuator. *Thin-Walled Structures*, 176, 109190.

[19] N.T. Phuong, D.T. Dong, C.V. Doan, V.H. Nam. (2022). Nonlinear buckling of higher-order shear deformable stiffened FG-GRC laminated plates with nonlinear elastic foundation subjected to combined loads. *Aerospace Science and Technology*, 127, 107736.

[20] V.H. Nam, D.T. Dong, C.V. Doan, N.T. Phuong. (2022). Nonlinear thermo-electro-mechanical buckling of higher-order shear deformable stiffened FG-GRC laminated plates. *International Journal of Applied Mechanics*, 14(06), 2250051.

[21] N.T. Phuong, D.T. Dong, C.V. Doan, V.H. Nam. (2023). Nonlinear buckling of stiffened FG-GRCL cylindrical panels under axial compression with the uniformly distributed temperature variation. *The European Physical Journal Plus*, 138(3), 234.

[22] V.H. Nam, D.T. Dong, C.V. Doan, N.T. Phuong. (2022). Nonlinear buckling of axially compressed FG-GRCL stiffened cylindrical panels with a piezoelectric layer by using Reddy's higher-order shear deformation theory. *Polymer Composites*, 43(11), 7952-7966.

[23] N.T. Phuong, C.V. Doan, V.H. Nam. (2023). Postbuckling analysis of externally pressured parabola, sinusoidal and cylindrical FG-GRCL panels using HSDT. *Journal of Science and Transport Technology*, 3(2), 34-42.

[24] V.H. Nam, C.V. Doan, N.T. Phuong. (2023). A new analytical approach to the nonlinear buckling and postbuckling behavior of functionally graded graphene reinforced composite laminated cylindrical, parabolic, and half-sinusoid shallow imperfect panels. *Polymer Composites*, 44(12), 8928-8945.

[25] S.W. Yang, Y.X. Hao, W. Zhang, L. Yang, L.T. Liu. (2021). Free vibration and buckling of eccentric rotating FG-GPLRC cylindrical shell using first-order shear deformation theory. *Composite Structures*, 263, 113728.

[26] Y. Wang, R. Zeng, M. Safarpour. (2022). Vibration analysis of FG-GPLRC annular plate in a thermal environment. *Mechanics Based Design of Structures and Machines*, 50(1), 352-370.

[27] N.T. Phuong, D.T. Dong, B.T. Tu, V.M. Duc, L.N. Khuong, P.T. Hieu, V.H. Nam. (2024). Nonlinear thermo-mechanical axisymmetric stability of FG-GPLRC spherical shells and circular plates resting on nonlinear elastic medium. *Ships and Offshore Structures*, 19(6), 820-830.

[28] L.N. Ly, B.T. Tu, D.T.N. Thu, D.T. Dong,

V.M. Duc, N.T. Phuong. (2022). Nonlinear thermo-mechanical buckling and postbuckling of sandwich FG-GPLRC spherical caps and circular plates with porous core by using higher-order shear deformation theory. Journal of Thermoplastic Composite Materials, 36(10), 089270572211478.

[29] C.V. Doan, V.H. Nam. (2022). Large Deflection Bending Analysis of FG-GPLRC Doubly Curved Thin Shallow Shells Stiffened by Oblique Stiffeners. *CIGOS 2021, Lecture Notes in Civil Engineering*, pp 351-360. *Springer, Singapore*.